Title

Developing a Targeted Quantitative Strategy for Sulfoxide-Containing MS-Cleavable Cross-Linked Peptides to Probe Conformational Dynamics of Protein Complexes

Journal

Analytical Chemistry, 94(10)

ISSN

0003-2700

Authors

Yu, Clinton
Wang, Xiaorong
Huang, Lan

Publication Date

2022-03-15

DOI

10.1021/acs.analchem.1c05298

Peer reviewed

HHS Public Access

Author manuscript

Anal Chem. Author manuscript; available in PMC 2022 April 11.

Published in final edited form as:

Anal Chem. 2022 March 15; 94(10): 4390–4398. doi:10.1021/acs.analchem.1c05298.

Developing a Targeted Quantitative Strategy for Sulfoxide-containing MS-cleavable Cross-linked Peptides to Probe Conformational Dynamics of Protein Complexes

Clinton Yu[1], **Xiaorong Wang**[1], **Lan Huang**[1,*]

[1]Department of Physiology & Biophysics, University of California, Irvine, Irvine, CA, 92694

Abstract

In recent years, cross-linking mass spectrometry (XL-MS) has made enormous strides as a technology for probing protein–protein interactions (PPIs) and elucidating architectures of multisubunit assemblies. To define conformational and interaction dynamics of protein complexes under different physiological conditions, various quantitative cross-linking mass spectrometry (QXL-MS) strategies based on stable isotope labeling have been developed. These QXL-MS approaches have effectively allowed comparative analysis of cross-links to determine their relative abundance changes at global scales. Although successful, it remains challenging to consistently obtain quantitative measurements on low-abundant cross-links. Therefore, targeted QXL-MS is needed to enable MS "Western" analysis of cross-links to enhance sensitivity and reliability in quantitation. To this end, we have established a robust parallel reaction monitoring (PRM)-based targeted QXL-MS platform using sulfoxide-containing MS-cleavable cross-linker disuccinimidyl sulfoxide (DSSO), permitting label-free comparative analysis of selected cross-links across multiple samples. In addition, we have applied this methodology to study phosphorylation-dependent conformational dynamics of the human 26S proteasome. The PRM-based targeted QXL-MS analytical platform described here is applicable for all sulfoxide-containing MS-cleavable cross-linkers and can be directly adopted for comparative studies of protein–protein interactions in various cellular contexts.

Graphical Abstract

*Correspondence should be addressed to Dr. Lan Huang (lanhuang@uci.edu), Medical Science I, D233, Department of Physiology & Biophysics, University of California, Irvine, Irvine, CA 92697-4560, Phone: (949) 824-8548, Fax: (949) 824-8540.

Supporting Information for Publication

The Supporting Information is available free of charge at https://pubs.acs.org/doi/10.1021/acs.analchem.1c05298. Additional experimental details, materials, and methods; supporting figures and legends describing the comparison of transition list schema and fluorogenic proteasomal activity assays (PDF).

26S proteasome subunit abundances (Table S1) (XLSX)

26S proteasome phosphopeptides and quantitation (Table S2) (XLSX)

List of unique 26S proteasome cross-links (Table S3) (XLSX)

K–K linkages mapped to the proteasome structure (PDB: 5GJR) (Table S4) (XLSX)

Quantitation and statistical analysis of cross-link abundances (Table S5) (XLSX)

COMPETING FINANCIAL INTERESTS

The authors declare no competing financial interests.

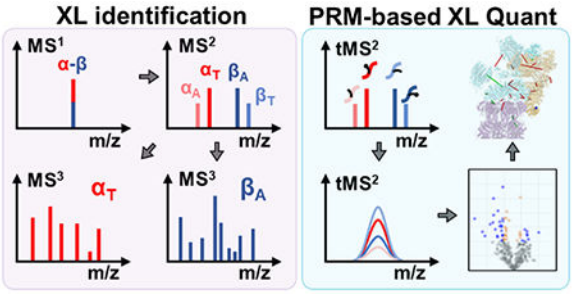

INTRODUCTION

Protein-protein interactions are central to the assembly of multi-subunit protein complexes, as well as the formation of intricate interaction networks that regulate cellular activity at the most fundamental level. Thus, a detailed understanding of these multimeric entities is critical for understanding their biological functions. Cross-linking mass spectrometry (XL-MS) has been instrumental in determining protein-protein interactions and architectures of large multi-protein assemblies [1–3]. Various XL-MS workflows have been established to facilitate the detection and identification of cross-linked peptides for systems-wide studies [4–10]. As dynamic entities, protein complexes often undergo molecular and structural changes in response to diverse cellular cues. To enable comparative analyses between multiple conformational states of proteins and protein complexes under different physiological conditions, multiple quantitative cross-linking mass spectrometry (QXL-MS) strategies have been developed [11,12]. Protein conformational changes can be assessed based on abundances of cross-linked peptides derived from the compared samples, which are typically quantified based on their relative spectral intensities at the MS^1 level. Thus, QXL-MS analysis is often accomplished by generating differentially labeled cross-linked peptides with either stable isotope-coded cross-linkers [4,13–18] or metabolic labeling of cross-linkable amino acids during cell culture [18–20]. In order to increase analysis throughput, the QMIX (Quantitation of Multiplexed, Isobaric-labeled cross (X)-linked peptides) method has been developed by integrating MS-cleavable cross-linkers with isobaric labeling reagents, enabling quantification of cross-links at the MS^n level for multiplexed QXL-MS studies [21]. While global quantitation methods have proven powerful and effective for discovery studies, these strategies mostly rely on data-dependent acquisition for peptide sampling during MS analysis, which often favor highly abundant peptides. Thus, alternative strategies are needed to improve sensitivity and precision in quantifying low abundance cross-linked peptides in complex matrices across compared samples.

In recent years, label-free quantitative methods have become a popular alternative in shotgun proteomics due to their potential to compare an unlimited number of samples. However, in comparison to stable isotope label-based methods, label-free quantitation requires each sample to be analyzed by MS separately, increasing both MS running time and experimental variance. To this end, data-independent acquisition (DIA) QXL-MS methods have been explored in limited protein studies and shown to increase the accuracy and reproducibility of cross-link quantitation [22]. Another strategy to improve accuracy and reliability of label-free measurements is targeted quantitation, which has been shown to

significantly enhance the detectability and sensitivity of selected peptide targets [23,24]. Similar to DIA-based approaches, targeted quantitation of peptides measures the relative abundances of their unique fragment ions at the MS^2 level, increasing analysis specificity with less interference from co-isolating/co-eluting ions that are often observed at the MS^1 level. Thus, selected reaction monitoring (SRM)-, multiple reaction monitoring (MRM)- and parallel reaction monitoring (PRM)-based targeted quantitation methods have been widely adopted in proteomics research as 'MS Western' assays for quantifying hundreds of peptides across multiple samples to monitor cellular pathways and validate potential biomarkers on a global scale [25,26]. One caveat in the application of PRM analysis to cross-linked peptides involves the generation of transition lists for targeted quantitation. In contrast to PRM analysis of non-cross-linked peptides, generating transition lists for conventional non-cleavable cross-linked peptides is challenging due to the difficulty in their unambiguous sequence identification. In comparison, PRM targeted quantitation would be better-suited for MS-cleavable cross-linked peptides due to their predictable and characteristic fragmentation independent of peptide sequence during MS^2 analysis [11,12]. The feasibility of PRM-based targeted quantitation of cross-linked peptides has been demonstrated by Bruce and colleagues with MS-cleavable PIR (protein interaction reporter) reagents and successfully applied to study *in vivo* protein interactions and their conformational response to drug treatment in cells [18,19]. While promising, whether the PRM-based strategy can be coupled with other MS-cleavable cross-linkers and generalized for QXL-MS studies has yet to be fully explored.

To facilitate the identification of cross-linked peptides, we have developed a series of sulfoxide-containing MS-cleavable cross-linkers targeting different residues (e.g. DSSO (disuccinimidyl sulfoxide)) [11,27–31]. These MS-cleavable reagents contain MS-labile C-S bonds that are selectively and preferentially fragmented prior to peptide backbone cleavage during CID, thus enabling simplified and accurate identification of cross-linked peptides by MS^n analysis. The established XL-MS platform has been successfully employed to elucidate architectures of protein complexes and define proteome-wide PPI landscapes *in vitro* and *in vivo* [9,11,28]. Given the success of sulfoxide-containing MS-cleavable reagents and their recent commercialization, it is beneficial to develop a PRM-based QXL-MS workflow to enable targeted quantitation of sulfoxide-containing cross-linked peptides for various biological applications. Here, we have developed a general PRM-QXL-MS workflow based on reliable and robust cross-link fragmentation of sulfoxide-containing MS-cleavable cross-linked peptides. Specifically, we have used DSSO to establish the strategy to generate PRM target and transition lists based on defined mass relationships between fragments and parent ions for sulfoxide-containing reagents [27]. The DSSO-based PRM-QXL-MS workflow has been successfully applied to quantify phosphorylation-dependent interaction and conformational changes within the human 26S proteasome. In total, we have identified and quantified 281 K-K linkages, and the results have provided new insights on phosphorylation-dependent regulation of the 26S proteasome. The same strategy can be directly adopted for other sulfoxide-containing MS-cleavable reagents-based XL-MS studies in the future.

EXPERIMENTAL PROCEDURES

Materials and Reagents

General chemicals for buffers and cell culture media were purchased from Fisher (Waltham, MA) or VWR (Radnor, PA). Sequencing grade trypsin was purchased from Promega Corp. (Madison, WI).

Affinity Purification of Human 26S Proteasomes and DSSO Cross-linking

Purification and cross-linking of human 26S proteasomes were prepared as previously described [20]. Stable 293 cell lines expressing HBTH-Rpn1 [32] were used and either treated with 50 nM calyculin for 30 min or left untreated and used as a control [33]. Details for affinity purification and cross-linking of proteasomes provided in Supplemental Methods.

LC MS/MS and Protein Quantification

Non-cross-linked peptides were identified by LC MS/MS analysis to assess the relative abundances of control and calyculin-treated proteasomes as previously described [20]. Quantitation of proteasome subunits in each sample were determined using MaxQuant [34] via LFQ and averaged across two biological replicates for each condition. Details provided in Supplemental Methods.

LC MS^n Analysis and Identification of 26S Proteasome Cross-links

Cross-linked peptides were identified by LC MS^n analysis as previously described [20]. Details for LC MS^n provided in Supplemental Methods.

Generation of PRM Library

To generate the targets for the PRM library, the theoretical *m/z* of all cross-link spectra matches (CSMs) were first calculated based on peptide composition and modifications. All CSMs for each unique target were then clustered and their respective elution times were used to determine their expected retention time windows. In order to generate a corresponding transition list for each of the unique PRM targets, the expected cross-link fragments were calculated based on the best-scoring CSM for each target. Specifically, the *m/z* of alkene (A)- and thiol (T)-modified cross-link fragments were calculated based on the charge distribution of the best scoring CSM, for a total of 4 transitions per cross-link α-β: α_A, α_T, β_A and β_T. In addition, a second scheme for determining the transition list was also tested, in which three charge distributions of cross-link fragments were calculated, resulting in a total of 12 transitions per PRM target. Two biological replicates were performed for each condition.

Targeted QXL-MS Analysis of the 26S Proteasome.

All cross-linked peptides identified from MS^n analysis of cross-linked proteasomes were selected for PRM targeted QXL-MS. Additionally, 10 heavy-labeled AQUA peptides were added as injection references for each sample. PRM target quantitation was performed in Skyline (21.1.0146, MacCoss Lab, UW) using the previously mentioned transition lists. The peak areas of all transitions were summed for each cross-link target, and then

further combined for cross-links corresponding to the same K-K linkage. Final cross-link abundances were then averaged across both biological replicates and compared between treated and control proteasomes. Details for PRM acquisition and Skyline quantitation provided in Supplemental Methods.

Proteolytic Activity Assay and Immunoblot

Proteasome activities were measured using fluorogenic peptide substrates SUC-LLVY-AMC, SUC-LLE-AMC, and SUC-ARR-AMC as described [35]. Details for proteolytic activity assay and immunoblot provided in Supplemental Methods.

RESULTS AND DISCUSSION

Developing a PRM-based Targeted QXL-MS Strategy for Sulfoxide-containing MS-cleavable Cross-linked Peptides

To determine interaction and conformational changes of protein complexes, we aimed to develop a PRM-based, label-free QXL-MS platform by integrating targeted quantitation with sulfoxide-containing MS-cleavable cross-linkers to enable comparative structural analyses. Since all sulfoxide-containing MS-cleavable cross-linkers yield cross-linked peptides that exhibit characteristically similar and predictable fragmentation during MS^2 analysis [11,27], we set out to establish the PRM-QXL-MS strategy using DSSO. As illustrated in Figure 1, due to the preferential cleavage of MS-cleavable C–S bonds during CID, the constituent peptides of a cross-link α-β are physically separated, yielding fragment ion pairs corresponding to peptides carrying alkene and sulfenic cross-linker fragment moieties (α_A/β_S and α_S/β_A) in MS^2. However, due to the preference of the sulfenic moiety to undergo hydrolysis to become a thiol during cross-linker fragmentation, the dominant fragment ions typically observed in MS^2 are alkene- and thiol-modified peptides (α_A/β_T and α_T/β_A) [27]. These MS^2 cross-link fragments are then selected and sequenced by MS^3 (Figure 1A) for unambiguous identification using conventional database searching tools. Finally, integration of MS^n data—the MS^1 parent ion, MS^2 fragment ions, and MS^3 peptide identifications—enables accurate and robust identification of cross-linked peptides.

Once the cross-link spectrum matches (CSMs) have been identified, simple calculations were utilized to generate the cross-linked peptide target list for PRM experiments. To create the cross-link target library, the theoretical parent *m/z* of each CSM was first calculated using the identified sequences and modifications of its constituent peptides. This facilitated the grouping of redundant CSMs by their *m/z* and peptide sequences. It also permitted the statistical determination of the expected retention time (RT) window of each cross-link target based on the elution times of its corresponding CSMs. The RT window for each target was centered based on the median retention time of all its identified CSMs, whereas the duration of the window was based on the distribution of RTs for those CSMs. Specifically, a ±2.5 min RT window was utilized if the median and average retention times for a group of CSMs were within 1 min of one another (98.3% of targets); ±3 min was used for the remaining targets. The target parameters for PRM acquisitions were set using the theoretical *m/z*, *z*, and RT values calculated in the previous step. For DSSO cross-linked peptides, PRM fragmentation was set to CID—as opposed to the commonly used HCD in targeted

quantitation (Figure 1B, *top left*)—in order to minimize backbone fragmentation and reduce the complexity of ions in the resulting targeted MS^2 (tMS^2) spectra (Figure 1B, *top right*). Overall, only a small portion (< 2%) of PRM targets exhibited a doublet or partially resolved peaks by LC separation, and most of them represent isobaric cross-linked products due to the presence of additional internal lysine(s) or ambiguous PTM sites within one or both cross-linked peptide constituents. In these situations, we considered the sum of both isobaric peaks for quantitation since isobaric positional cross-link isomers contain identical peptide sequences describing the same interaction regions.

Automated quantitation of the cross-links from PRM spectra requires the generation of a transition list containing the expected fragments associated with each cross-link target. The theoretical *m/z* values for cross-link fragments were directly calculated using the peptide sequence, post-translational modifications, and potential cross-linker remnant moieties. As alkene- and thiol-modified peptide fragments are most prominent during MS^2 analysis of DSSO cross-linked peptides, a 4-fragment scheme reflecting the best-scoring CSM for each target was employed for transition calculations. Once the transition lists were generated, we used Skyline to quantify the cross-links in each PRM experiment [24].

Establishing the PRM-QXL-MS Workflow to Study Phosphorylation-dependent Structural Dynamics of the 26S Proteasome

To establish the PRM-QXL-MS workflow for studying protein complexes, we applied the targeted quantitation method to determine phosphorylation-dependent interaction and structural dynamics of the human 26S proteasome, a macromolecular machine responsible for ubiquitin/ATP dependent protein degradation. The 26S proteasome is composed of two subcomplexes: the 20S core particle (CP) and the 19S regulatory particle (RP) [36]. The 20S CP is formed by 14 different subunits (7α and 7β) arranged in an evolutionarily conserved, barrel-like structure of four stacked heptameric rings in the order αββα. The 19-subunit 19S RP flanks either or both ends of the 20S CP and can be further divided into the 19S ‘base’ and ‘lid’ subcomplexes. In recent years, numerous studies have shown that the structure and function of the 26S proteasome is tightly regulated by multiple post-translational mechanisms [37,38]. In particular, proteasome phosphorylation has been identified as a key regulatory mechanism in modulating proteasomal activities, which has displayed great therapeutic potential in various diseases including neurodegenerative disorders [39,40]. However, the molecular details underlying phosphorylation-dependent regulation of proteasomal activity remain elusive.

In order to explore the molecular details underlying phosphorylation-dependent regulation of 26S proteasomes, we have performed comparative structural analyses of the 26S proteasome complex by PRM-based targeted quantitation (Figure 2). To this end, we have employed a CRISPR/Cas9-engineered 293 cell line stably expressing an HBTH-tagged 19S subunit Rpn1 (i.e. $293^{HBTH\text{-}Rpn1}$ cells) to isolate proteasome complexes for analysis [32]. To better maintain the intactness of the 26S proteasome complex during native purification, mild *in vivo* formaldehyde was carried out prior to cell lysis [41]. To determine phosphorylation-dependent molecular changes, one population of cells was treated with protein phosphatase inhibitor calyculin A to preserve proteasome phosphorylation, while untreated cells were

used as a control. Proteasome complexes were then purified from equivalent amounts of treated and untreated cells separately using 1-step HB tag-based purification by binding to streptavidin, followed by DSSO cross-linking on-bead and subsequent trypsin digestion [33]. The resulting peptide digests were first analyzed using LC MS/MS to determine calyculin-dependent changes in proteasome composition and phosphorylation (Figure 2, *path I*). LC MS^n analysis was then performed to identify cross-linked peptides (Figure 2, *path II*) and build an XL target library for PRM-QXL-MS analysis of the 26S proteasome to delineate phosphorylation-dependent changes (Figure 2, *path III*).

Characterization of Proteasome Assembly and Phosphorylation by LC MS/MS

In this work, LC MS/MS analysis of the purified 26S proteasomes identified a total of 32 proteasomal subunits, whose relative abundances in treated and untreated samples were determined based on LFQ values using MaxQuant (Figure 3A, Supplemental Table S1). Correlation plots of subunit abundances indicated high data reproducibility from biological replicates of control and treated samples, respectively (Figure 3B, C). Next, we employed the average LFQ ratios for 19S and 20S subunits to estimate the relative abundances of the 19S and 20S subcomplexes in the two compared samples (Figure 3A). As a result, while the relative abundance of 19S was unchanged, the abundance of 20S subcomplex in treated samples was consistently ~25% higher compared to untreated control samples. These results suggest that *in vivo* calyculin A treatment promotes increased 26S proteasome assembly (Supplemental Figure 1).

To understand whether proteasome phosphorylation was changed during calyculin treatment, we identified and quantified 12 phosphorylated peptides describing 10 phosphosites from 5 proteasome subunits (Rpn1-2, 6, 10, Rpt2) at the MS^1 level using Skyline (Supplemental Table S2). While the proteasome has been associated with over 400 phosphosites [38], most of them were determined by high-throughput experiments utilizing enrichment of phosphopeptides from entire proteomes encompassing compositionally heterogenous proteasomes. Here, the phosphosites were identified from direct analysis of affinity purified Rpn1-containing 26S proteasome without phosphoenrichment, signifying the most abundant phosphorylation within the complex. These phosphosites were collapsed into 8 groups based on their proximity and peptide sequence identifications: Rpn1:S16, Rpn1:S361, Rpn2:T273|T276, Rpn2:T311, Rpn2:T830, Rpn6:S14, Rpn10:T264|S266, and Rpt2:S6, all of which have been previously reported [38]. In total, only 3 groups of phosphoresidues appeared to display enhanced phosphorylation (~2-10-fold increase) in calyculin-treated samples (Rpn2:T311, Rpn6:S14, and Rpn10:T264|S266). Since calyculin is expected to inhibit PP1 and PP2A phosphatases, our results suggest that Rpn2, Rpn6, and Rpn10 carry PP1- or PP2A-regulated phosphorylation sites. Interestingly, while the two of the three innate proteasomal ubiquitin receptors (Rpn1, Rpn10 and Rpn13) were found to be phosphorylated, Rpn1 phosphorylation did not appear to be impacted by calyculin treatment. Among the three changed phosphorylation sites, Rpn6:S14 appeared to have the most significantly increased phosphorylation in response to calyculin treatment. Previous reports have shown that PKA-mediated phosphorylation of Rpn6:S14 is biologically significant as it increases proteasome assembly and proteolytic activities [38,40]. Therefore, we suspect that the

enhanced proteasome assembly observed here is most likely attributed to phosphorylation of Rpn6:S14.

Identification of DSSO Cross-linked Peptides of the 26S Proteasome

To understand phosphorylation-mediated changes, we performed DSSO-based XL-MS analysis of the 26S proteasome using LC MS^n [27]. This yielded the identification of 3,532 total CSMs, representing 414 unique cross-linked peptides describing 288 unique K-K linkages within the 26S proteasome (Supplemental Table S3). Of these, 117, 85, and 43 represent intra- and inter-subunit linkages within the 19S base, 19S lid, and 20S, respectively. The remaining 46 cross-links represent inter-subcomplexes linkages (19 base-lid, 19 base-20S, 1 lid-20S) (Figure 4A). To evaluate the validity of the identified cross-links, we first mapped them to a high-resolution cryo-EM structure (PDB: 5GJR) of the human 26S proteasome [42] to assess residue proximities (Figure 4B). Due to missing densities, only 238 of 288 K-K linkages were mapped, in which 92.0% (225/238) were satisfied within the maximum Cα-Cα distance threshold (< 30 Å) spanned by DSSO (Figure 4C, Supplemental Table S3) [33]. Collectively, our results support the validity of proteasome cross-links identified here.

PRM-QXL-MS Analysis of the 26S Proteasome

To build the XL library for targeted quantitation, the theoretical *m/z* values for each of the 414 unique cross-link targets for PRM experiments were calculated. Here, two biological replicates of control and calyculin-treated samples were analyzed (Figure 1A). As discussed above, four transition ions (α_A, α_T, β_A, β_T) were measured for quantitation of each cross-link target. As an example, Figure 5A displays the respective peak profiles detected for four transition ions ($\alpha_A^{2+}/\alpha_T^{2+}$, $\beta_A^{2+}/\beta_T^{2+}$) corresponding to peptide fragments of the inter-subunit cross-link: Rpn2:K574-Rpn8:K28 (*m/z* 465.0035^{4+}). Based on the summed peak areas of these transition ions, the relative abundance ratio of this cross-linked peptide between treated and control samples was determined to be approximately 1.0—suggesting no significant change (Figure 5A). In comparison, PRM analysis of the inter-subunit cross-link Rpn1:K39-Rpt6:K330 (*m/z* 500.7589^{4+}) determined its relative abundance ratio (treated/control) to be 0.4, suggesting a decrease of 60% after calyculin treatment (Figure 5B). Among the 414 targets, 412 were reliably quantified, whereas 2 were not due to low signal or unexpected elution shift during data acquisition. This strategy was proven to be beneficial for improving detection and quantitation accuracy of cross-links, as conventional quantitation performed at the MS^1 level was observed to yield significantly more missing and/or inaccurate values due to differences in detectability and background interference—particularly for low-abundance cross-links. We then summed the normalized results of cross-linked peptides describing the same residue-to-residue linkage, yielding quantitative values for a total of 281 unique K-K linkages.

To assess the reproducibility of PRM-based quantitation, we employed linear regression analyses to compare the normalized abundances of all cross-links between the two biological replicates of each sample. As a result, regression plots for both control (Figure 5C) and treated samples (Figure 5D) displayed a strong linear relationship, demonstrating high reproducibility between these biological replicates. Thus, average abundances of cross-link

targets were used to calculate their quantitative ratios between treated and untreated samples. These ratios were then binned, and the distribution plotted as a histogram (Figure 5E). Overall, the histogram displayed a normal distribution centered at zero indicating that most cross-links were unaffected. The standard deviation of the dataset was determined to be 0.55, nearly identical to 1σ as determined through the conventional heuristic that 68% of all values lie within one standard deviation of the mean (cut-off: 0.554).

Comparison of 4-Fragment and 12-Fragment Transitions in Quantitative Analysis

While quadruply charged cross-link species would typically be expected to split evenly into pairs of doubly charged fragment ions, differential charge splitting can occur during the fragmentation of cross-linked peptides in MS^2, resulting in more than four major fragments. This observation often occurs for cross-linked peptides with charges greater than 4+. To determine whether considering more transition ions would improve quantitation accuracy, we re-analyzed the PRM experiments using a 12-fragment scheme consisting of three sets of four transitions: one set based on the best-scored CSM, and two additional sets with charges offset by 1. For example, in the previous examples which only considered pairs of double-charged transitions ($\alpha_A^{2+}/\alpha_T^{2+}$, $\beta_A^{2+}/\beta_T^{2+}$) from a quadruply charged parent, the second scheme would additionally sample transition pairs $\alpha_A^{+}/\alpha_T^{+}$, $\beta_A^{3+}/\beta_T^{3+}$ as well as $\alpha_A^{3+}/\alpha_T^{3+}$, β_A^{+}/β_T^{+}. Quantitation of the 412 cross-link targets was repeated using this 12-fragment transition scheme. Based on the correlation plot of treated/control abundance ratios obtained using the two transition strategies (4-fragment vs. 12-fragment) for PRM quantitation (Supplemental Figure 2), the differences in abundance ratios afforded by each strategy were minimal. In fact, attempting to account for additional transition ions for each PRM target appeared to introduce artifact data points that required manual removal, or else resulted in outlier ratios. Thus, the final quantitative ratios for cross-links were only derived from the 4-fragment transition scheme. As calyculin-induced phosphorylation only enhances proteasome assembly by ~25%, we expected the observable conformational changes in the 26S proteasomes under our experimental conditions to be subtle. In total, 90 of 281 K-K linkages were found to exhibit a change in cross-link abundance greater than 1σ (~1.5-fold) when comparing between treated and control proteasomes. These linkages were considered as significantly changed for further analysis.

Mapping Phosphorylation-dependent Cross-links

To evaluate the accuracy of the changed K-K linkages, we calculated their p-values using a two-tailed, Student's t-distribution with unpaired, unequal variance. Linkages with a $\log_2$ change greater than one standard deviation and p-value < 0.1 were classified as statistically changed (Figure 6A). The application of a p-value filter reduced the number of statistically changed K-K linkages from 90 to 31. Among them, the abundances of 9 K-K linkages were shown to be increased (1.55 ~ 2.50-fold) in response to calyculin treatment, whereas the remaining 22 were reduced (1.56 ~ 3.21-fold). The good correlation between biological replicates (R^2 of 0.9997 and average CV of 10.1% for control samples, R^2 of 0.9996 and average CV of 12.5% for calyculin-treated samples) further suggests the observed cross-link changes most likely describe the expected conformational changes in the complex and are not attributed to experimental variability. Since none of the phosphorylated residues were identified within the sequences covered by cross-linked peptides and only

a few phosphosites are specifically modulated by calyculin, the observed changes in K-K linkage abundances are most likely attributed to conformational changes due to increased phosphorylation.

We first categorized the 31 changed K-K linkages based on their subcomplex localization and mapped them onto the high-resolution structure (Figure 6B, C), resulting in eight 19S lid-lid, fourteen 19S base-base, four 19S lid-base, four 20S-20S and one 20S-19S cross-link. Among the 19S lid-lid cross-links, 5 involve either Rpn6—which has been described as a 'molecular clamp' that holds the 19S and 20S subcomplexes together [43]—or Rpn5, which has been shown to interact and potentially interface with Rpn6 through their PCI domains. Interestingly, all 5 of those linkages were shown to decrease as a result of Rpn6 phosphorylation, despite the cross-linked lysines being distant from the S14 phosphorylation site. Specifically, the cross-linked residues of Rpn5 (K212, K301, K330, K441) and Rpn6 (K205, K223, K325) were found to be in or proximal to their PCI domains, indicating these regions as potential ones that undergo conformational changes in response to phosphorylation of Rpn6. Changes in cross-link abundance within the 19S lid were also observed involving Rpn8 and Rpn9 of the 19S lid, which favored calyculin treatment. While this may be related to the phosphorylation of Rpn10 due to the proximity of the proteins, the Rpn10 phosphosite was not resolved in the current structure due to missing regions.

The most structural movement observed within the proteasome was centered around the 19S base, which was implicated in 18 changed linkages. Of these, 15 were shown to decrease in abundance, in which 10 involved the C-terminal domains of 4 ATPase subunits (Rpt2-4, 6). As the C-termini of these proteasomal ATPases function as keys to induce gate-opening and allow substrate entry into the 20S [44], it is possible that changes in this region would be associated with activation of proteasomal degradation. Mapping of these decreased cross-links suggests that the upregulated proteasomal activity associated with increased phosphorylation due to calyculin treatment may be related to the gate opening mechanism exhibited by the ATPase ring. Interestingly, cross-links involving Rpt1 were uniquely shown to increase following calyculin treatment; two cross-links involved the C-terminal regions of Rpt1, one intramolecular cross-link with itself—Rpt1:K181-Rpt1:K356—and the other an inter-subunit cross-link to 20S subunit α4 through an N-terminal residue near the pockets associated with gate opening, Rpt1:K418-α4:K27. The observed increase of this 19S base-20S cross-link further suggests a close interaction between the 19S base and 20S that is upregulated by calyculin treatment. While it remains difficult to pinpoint the structural rationales that result in changed cross-links due to various potential factors, our results do suggest that phosphorylation-dependent conformational changes within the 26S proteasome are able to be quantified and determined through PRM-based QXL-MS.

Biochemical Validation of Phosphorylation-dependent Regulation of the 26S Proteasome

To evaluate the biological effect of calyculin treatment on proteasome function, we measured proteolytic activities of 26S proteasomes purified from treated and control cells. As a result, the chymotrypsin-, trypsin- and caspase-like activities of 26S proteasomes were increased in response to calyculin treatment (Supplemental Figure 3), confirming that increased phosphorylation enhances proteasomal activities as previously reported [38]. Due to

the significantly augmented phosphorylation at S14 of Rpn6 triggered by calyculin treatment and its known biological significance [39,40], we suspect that this phosphorylation is central to the enhanced assembly and conformational changes of the 26S proteasomes observed here. This work presents a general analytical workflow for us to further dissect molecular changes underlying the regulation of the 26S proteasome under various biological conditions in the future.

CONCLUSION

Here, we have developed a PRM-based targeted QXL-MS platform using DSSO cross-linked peptides, which has been successfully applied to define phosphorylation-dependent conformational changes of the 26S proteasome. Through this process, we have identified subunits and regions that may reflect conformational changes associated with the upregulation of proteasomal activity associated with increased phosphorylation. Importantly, this PRM-QXL-MS strategy is directly applicable for all sulfoxide-based MS-cleavable cross-linking reagents and can also be extended to other MS-cleavable cross-linkers. Moreover, targeted quantitation enhances the sensitivity and detection of cross-linked species compared to QXL-MS strategies measuring cross-link abundance at the MS^1 level [45]. This is particularly beneficial for quantifying low-abundance cross-links which are not uniformly detectable across all biological replicates, resulting in fewer overall missing values. The quantification of each cross-link based on specific fragment ions may also improve quantitation accuracy by reducing signal contamination by co-eluting ions with similar *m/z.* Thus, the PRM-based targeted QXL-MS method established here can be used as an “MS structural Western” to facilitate future studies on conformational dynamics of protein complexes under different biological conditions.

Supplementary Material

Refer to Web version on PubMed Central for supplementary material.

ACKNOWLEDGMENT

We thank Drs. A.L. Burlingame, Robert Chalkley and Peter Baker for the support of Protein Prospector. This work was supported by National Institutes of Health grants R01GM074830 and R01GM130144 to L.H.

ABBREVIATIONS

19S RP	19S regulatory particle
20S CP	20S core particle
CSM	Crosslink spectrum match
DSSO	Disuccinimidyl sulfoxide
HCD	Higher-energy collision-induced dissociation
LC MS/MS	Liquid chromatography-coupled tandem mass spectrometry
LC MS^n	Liquid chromatography-coupled multistage mass spectrometry

PPIs	Protein-protein interactions
PRM	Parallel reaction monitoring
QXL-MS	Quantitative cross-linking mass spectrometry
tMS^2	Targeted tandem mass spectrometry
XL-MS	Cross-linking mass spectrometry

REFERENCES

(1). Lasker K; Forster F; Bohn S; Walzthoeni T; Villa E; Unverdorben P; Beck F; Aebersold R; Sali A; Baumeister W Molecular architecture of the 26S proteasome holocomplex determined by an integrative approach Proc Natl Acad Sci U S A 2012, 109, 1380–1387. [PubMed: 22307589]

(2). Erzberger JP; Stengel F; Pellarin R; Zhang S; Schaefer T; Aylett CH; Cimermancic P; Boehringer D; Sali A; Aebersold R; Ban N Molecular architecture of the 40SeIF1eIF3 translation initiation complex Cell 2014, 158, 1123–1135. [PubMed: 25171412]

(3). Shi Y; Fernandez-Martinez J; Tjioe E; Pellarin R; Kim SJ; Williams R; Schneidman D; Sali A; Rout MP; Chait BT Structural characterization by cross-linking reveals the detailed architecture of a coatomer-related heptameric module from the nuclear pore complex Mol Cell Proteomics 2014, 13, 2927–2943. [PubMed: 25161197]

(4). Tan D; Li Q; Zhang MJ; Liu C; Ma C; Zhang P; Ding YH; Fan SB; Tao L; Yang B; Li X; Ma S; Liu J; Feng B; Liu X; Wang HW; He SM; Gao N; Ye K; Dong MQ, et al. Trifunctional cross-linker for mapping protein-protein interaction networks and comparing protein conformational states eLife 2016, 5.

(5). Klykov O; Steigenberger B; Pektas S; Fasci D; Heck AJR; Scheltema RA Efficient and robust proteome-wide approaches for cross-linking mass spectrometry Nat Protoc 2018, 13, 2964–2990. [PubMed: 30446747]

(6). Iacobucci C; Gotze M; Ihling CH; Piotrowski C; Arlt C; Schafer M; Hage C; Schmidt R; Sinz A A cross-linking/mass spectrometry workflow based on MS-cleavable cross-linkers and the MeroX software for studying protein structures and protein-protein interactions Nat Protoc 2018, 13, 2864–2889. [PubMed: 30382245]

(7). Chavez JD; Mohr JP; Mathay M; Zhong X; Keller A; Bruce JE Systems structural biology measurements by in vivo cross-linking with mass spectrometry Nat Protoc 2019, 14, 2318–2343. [PubMed: 31270507]

(8). Yugandhar K; Wang TY; Leung AK; Lanz MC; Motorykin I; Liang J; Shayhidin EE; Smolka MB; Zhang S; Yu H MaXLinker: Proteome-wide Cross-link Identifications with High Specificity and Sensitivity Mol Cell Proteomics 2020, 19, 554–568. [PubMed: 31839598]

(9). Wheat A; Yu C; Wang X; Burke AM; Chemmama IE; Kaake RM; Baker P; Rychnovsky SD; Yang J; Huang L Protein interaction landscapes revealed by advanced in vivo cross-linking-mass spectrometry Proc Natl Acad Sci U S A 2021, 118.

(10). Rey M; Dhenin J; Kong Y; Nouchikian L; Filella I; Duchateau M; Dupre M; Pellarin R; Dumenil G; Chamot-Rooke J Advanced In Vivo Cross-Linking Mass Spectrometry Platform to Characterize Proteome-Wide Protein Interactions Anal Chem 2021, 93, 4166–4174. [PubMed: 33617236]

(11). Yu C; Huang L Cross-Linking Mass Spectrometry: An Emerging Technology for Interactomics and Structural Biology Anal Chem 2018, 90, 144–165. [PubMed: 29160693]

(12). Wippel HH; Chavez JD; Tang X; Bruce JE Quantitative interactome analysis with chemical cross-linking and mass spectrometry Curr Opin Chem Biol 2021.

(13). Fischer L; Chen ZA; Rappsilber J Quantitative cross-linking/mass spectrometry using isotope-labelled cross-linkers Journal of proteomics 2013, 88, 120–128. [PubMed: 23541715]

(14). Schmidt M; Finley D Regulation of proteasome activity in health and disease Biochim Biophys Acta 2014, 1843, 13–25. [PubMed: 23994620]

(15). Kukacka Z; Rosulek M; Strohalm M; Kavan D; Novak P Mapping protein structural changes by quantitative cross-linking Methods 2015, 89, 112–120. [PubMed: 26048481]

(16). Chen Z; Fischer L; Tahir S; Bukowski-Wills JC; Barlow P; Rappsilber J Quantitative cross-linking/mass spectrometry reveals subtle protein conformational changes Wellcome open research 2016, 1, 5. [PubMed: 27976756]

(17). Yu C; Mao H; Novitsky EJ; Tang X; Rychnovsky SD; Zheng N; Huang L Gln40 deamidation blocks structural reconfiguration and activation of SCF ubiquitin ligase complex by Nedd8 Nature communications 2015, 6, 10053.

(18). Zhong X; Navare AT; Chavez JD; Eng JK; Schweppe DK; Bruce JE Large-Scale and Targeted Quantitative Cross-Linking MS Using Isotope-Labeled Protein Interaction Reporter (PIR) Cross-Linkers J Proteome Res 2017, 16, 720–727. [PubMed: 28152603]

(19). Chavez JD; Eng JK; Schweppe DK; Cilia M; et al. PLoS One 2016, 11 (12), e0167547. [PubMed: 27997545]

(20). Yu C; Wang X; Huszagh AS; Viner R; Novitsky E; Rychnovsky SD; Huang L Probing H2O2-mediated Structural Dynamics of the Human 26S Proteasome Using Quantitative Cross-linking Mass Spectrometry (QXL-MS) Mol Cell Proteomics 2019, 18, 954–967. [PubMed: 30723094]

(21). Yu C; Huszagh A; Viner R; Novitsky EJ; Rychnovsky SD; Huang L Developing a Multiplexed Quantitative Cross-Linking Mass Spectrometry Platform for Comparative Structural Analysis of Protein Complexes Anal Chem 2016, 88, 10301–10308. [PubMed: 27626298]

(22). Muller F; Graziadei A; Rappsilber J Quantitative Photo-crosslinking Mass Spectrometry Revealing Protein Structure Response to Environmental Changes Anal Chem 2019, 91, 9041–9048. [PubMed: 31274288]

(23). Peterson AC; Russell JD; Bailey DJ; Westphall MS; Coon JJ Parallel reaction monitoring for high resolution and high mass accuracy quantitative, targeted proteomics Mol Cell Proteomics 2012, 11, 1475–1488. [PubMed: 22865924]

(24). Rauniyar N Parallel Reaction Monitoring: A Targeted Experiment Performed Using High Resolution and High Mass Accuracy Mass Spectrometry Int J Mol Sci 2015, 16, 28566–28581. [PubMed: 26633379]

(25). Shi T; Song E; Nie S; Rodland KD; Liu T; Qian WJ; Smith RD Advances in targeted proteomics and applications to biomedical research Proteomics 2016, 16, 2160–2182. [PubMed: 27302376]

(26). Kumar V; Ray S; Ghantasala S; Srivastava S An Integrated Quantitative Proteomics Workflow for Cancer Biomarker Discovery and Validation in Plasma Frontiers in oncology 2020, 10, 543997. [PubMed: 33072574]

(27). Kao A; Chiu CL; Vellucci D; Yang Y; Patel VR; Guan S; Randall A; Baldi P; Rychnovsky SD; Huang L Development of a novel cross-linking strategy for fast and accurate identification of cross-linked peptides of protein complexes Mol Cell Proteomics 2011, 10, M110.002212.

(28). Kaake RM; Wang X; Burke A; Yu C; Kandur W; Yang Y; Novtisky EJ; Second T; Duan J; Kao A; Guan S; Vellucci D; Rychnovsky SD; Huang L A New In Vivo Cross-linking Mass Spectrometry Platform to Define Protein-Protein Interactions in Living Cells Mol Cell Proteomics 2014, pii: mcp.M114.042630.

(29). Gutierrez CB; Block SA; Yu C; Soohoo SM; Huszagh AS; Rychnovsky SD; Huang L Development of a Novel Sulfoxide-Containing MS-Cleavable Homobifunctional Cysteine-Reactive Cross-Linker for Studying Protein-Protein Interactions Anal Chem 2018, 90, 7600–7607. [PubMed: 29792801]

(30). Gutierrez C; Chemmama IE; Mao H; Yu C; Echeverria I; Block SA; Rychnovsky SD; Zheng N; Sali A; Huang L Structural dynamics of the human COP9 signalosome revealed by cross-linking mass spectrometry and integrative modeling Proc Natl Acad Sci U S A 2020, 117, 4088–4098. [PubMed: 32034103]

(31). Gutierrez C; Salituro LJ; Yu C; Wang X; DePeter SF; Rychnovsky SD; Huang L Enabling Photoactivated Cross-Linking Mass Spectrometric Analysis of Protein Complexes by Novel MS-Cleavable Cross-Linkers Mol Cell Proteomics 2021, 20, 100084. [PubMed: 33915260]

(32). Lin DW; Chung BP; Huang JW; Wang X; Huang L; Kaiser P Microhomology-based CRISPR tagging tools for protein tracking, purification, and depletion The Journal of biological chemistry 2019, 294, 10877–10885. [PubMed: 31138654]

(33). Wang X; Cimermancic P; Yu C; Schweitzer A; Chopra N; Engel JL; Greenberg C; Huszagh AS; Beck F; Sakata E; Yang Y; Novitsky EJ; Leitner A; Nanni P; Kahraman A; Guo X; Dixon JE; Rychnovsky SD; Aebersold R; Baumeister W, et al. Molecular Details Underlying Dynamic Structures and Regulation of the Human 26S Proteasome Mol Cell Proteomics 2017, 16, 840–854. [PubMed: 28292943]

(34). Cox J; Matic I; Hilger M; Nagaraj N; Selbach M; Olsen JV; Mann M A practical guide to the MaxQuant computational platform for SILAC-based quantitative proteomics Nat Protoc 2009, 4, 698–705. [PubMed: 19373234]

(35). Yu C; Wang X; Li W; Liu Y; Huang L Developing a Bimolecular Affinity Purification Strategy to Isolate 26S Proteasome Holocomplexes for Complex-Centric Proteomic Analysis Anal Chem 2021, 93, 13407–13413. [PubMed: 34550675]

(36). Voges D; Zwickl P; Baumeister W The 26S proteasome: a molecular machine designed for controlled proteolysis. Annu Rev Biochem. 1999, 68, 1015–1068. [PubMed: 10872471]

(37). Collins GA; Goldberg AL The Logic of the 26S Proteasome Cell 2017, 169, 792–806. [PubMed: 28525752]

(38). Guo X; Huang X; Chen MJ Reversible phosphorylation of the 26S proteasome Protein & cell 2017, 8, 255–272. [PubMed: 28258412]

(39). Lokireddy S; Kukushkin NV; Goldberg AL cAMP-induced phosphorylation of 26S proteasomes on Rpn6/PSMD11 enhances their activity and the degradation of misfolded proteins Proc Natl Acad Sci U S A 2015, 112, E7176–7185. [PubMed: 26669444]

(40). Myeku N; Clelland CL; Emrani S; Kukushkin NV; Yu WH; Goldberg AL; Duff KE Tau-driven 26S proteasome impairment and cognitive dysfunction can be prevented early in disease by activating cAMP-PKA signaling Nat Med 2016, 22, 46–53. [PubMed: 26692334]

(41). Yu C; Yang Y; Wang X; Guan S; Fang L; Liu F; Walters KJ; Kaiser P; Huang L Characterization of Dynamic UbR-Proteasome Subcomplexes by In vivo Cross-linking (X) Assisted Bimolecular Tandem Affinity Purification (XBAP) and Label-free Quantitation Mol Cell Proteomics 2016, 15, 2279–2292. [PubMed: 27114451]

(42). Huang X; Luan B; Wu J; Shi Y An atomic structure of the human 26S proteasome Nat Struct Mol Biol 2016, 23, 778–785. [PubMed: 27428775]

(43). Pathare GR; Nagy I; Bohn S; Unverdorben P; Hubert A; Korner R; Nickell S; Lasker K; Sali A; Tamura T; Nishioka T; Forster F; Baumeister W; Bracher A The proteasomal subunit Rpn6 is a molecular clamp holding the core and regulatory subcomplexes together Proc Natl Acad Sci U S A 2012, 109, 149–154. [PubMed: 22187461]

(44). Polpitiya AD; Qian WJ; Jaitly N; Petyuk VA; Adkins JN; Camp DG 2nd; Anderson GA; Smith RD DAnTE: a statistical tool for quantitative analysis of-omics data Bioinformatics 2008, 24, 1556–1558. [PubMed: 18453552]

(45). Chen ZA; Rappsilber J Quantitative cross-linking/mass spectrometry to elucidate structural changes in proteins and their complexes Nat Protoc 2019, 14, 171–201. [PubMed: 30559374]

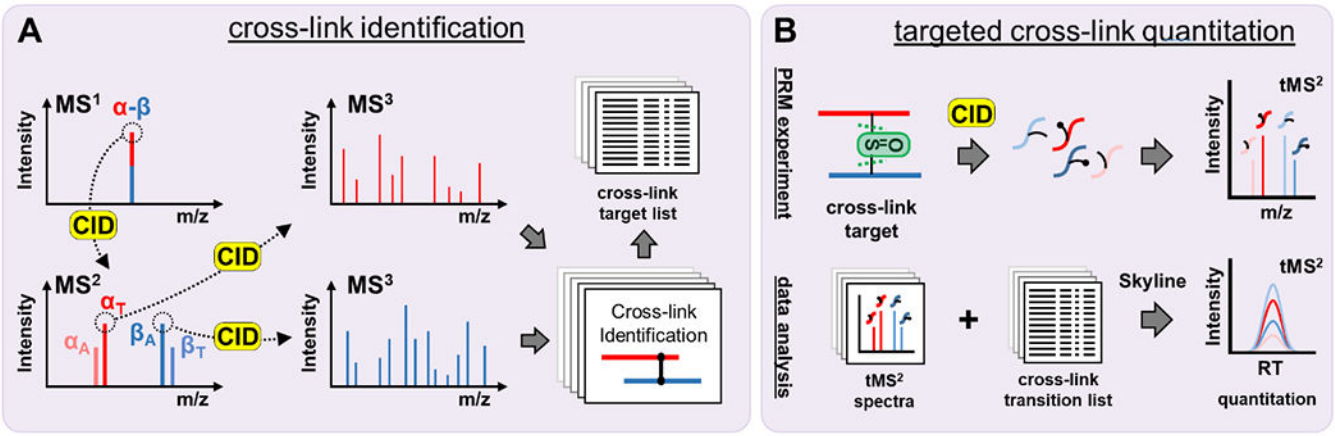

Figure 1. General workflow for cross-link identification and targeted cross-link quantitation.

(A) Cross-links are identified by LC MS^n, and the resulting cross-link spectral matches are used to develop a target library and transition list for PRM analysis. **(B)** Cross-links are analyzed by targeted PRM analysis using CID to produce cross-link fragments while minimizing backbone fragmentation, simplifying the quantitation process. Transitions for each cross-link target are measured in Skyline.[19]

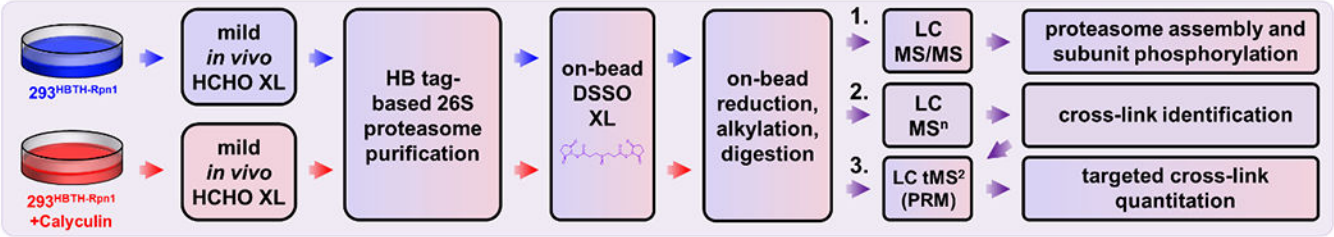

Figure 2. Workflow for investigating calyculin-dependent conformational dynamics of the 26S proteasome.

26S proteasomes were purified from control and calyculin-treated $293^{HTBH\text{-}Rpn1}$ cells and cross-linked. Digested cross-linked peptides were then analyzed by LC MS/MS, LC MS^n, and PRM to determine proteasomal subunit abundances, phosphorylation, and cross-link identification and quantitation.

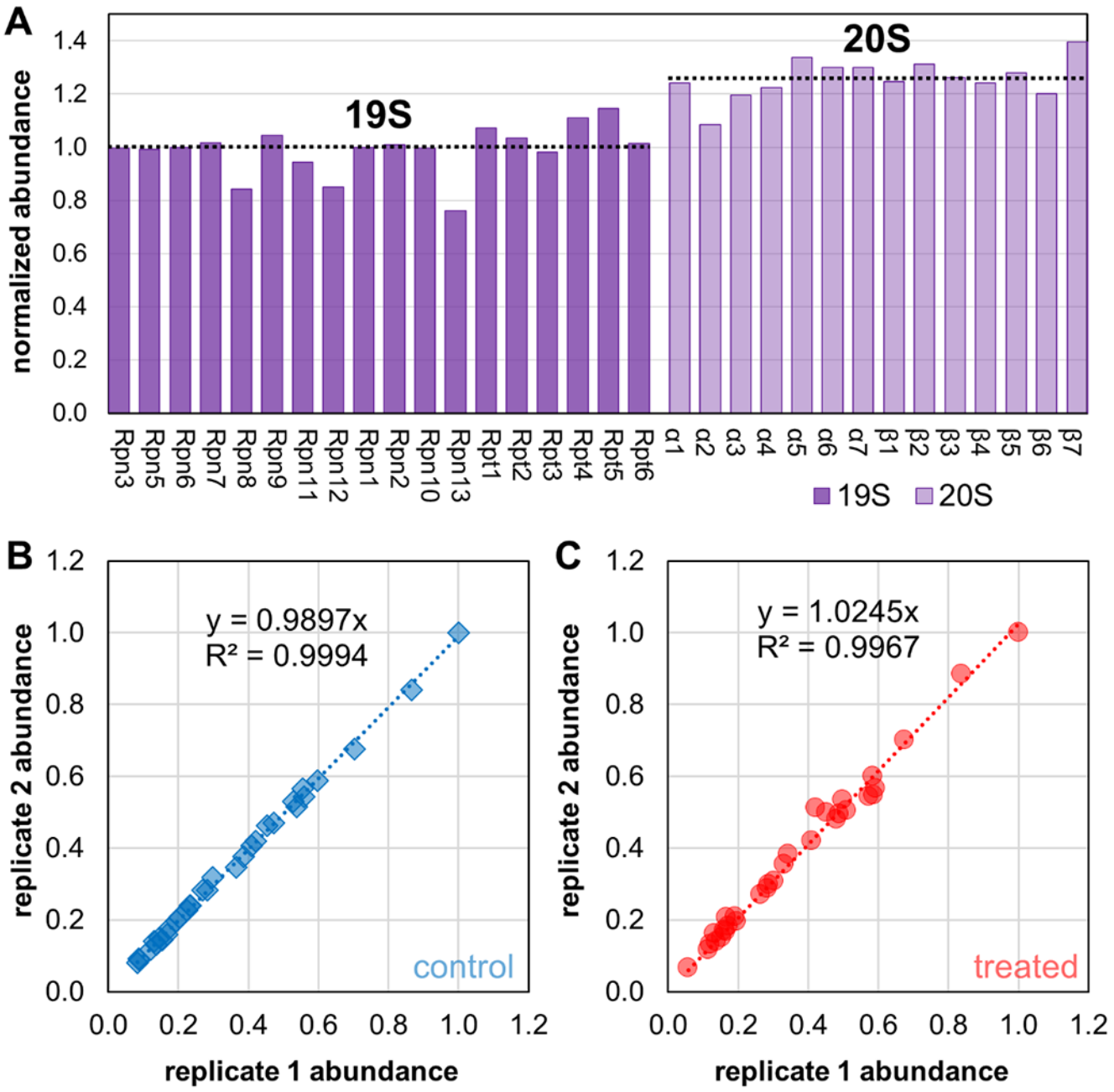

Figure 3. Quantitation of purified 26S proteasomes.

(A) Relative abundance ratios (treated/control) of proteasome subunits as determined by LFQ measurements in MaxQuant. All subunit abundances normalized to Rpn1. Pair-wise correlation plots between **(B)** control replicates and **(C)** calyculin-treated replicates indicating good agreement between replicate experiments.

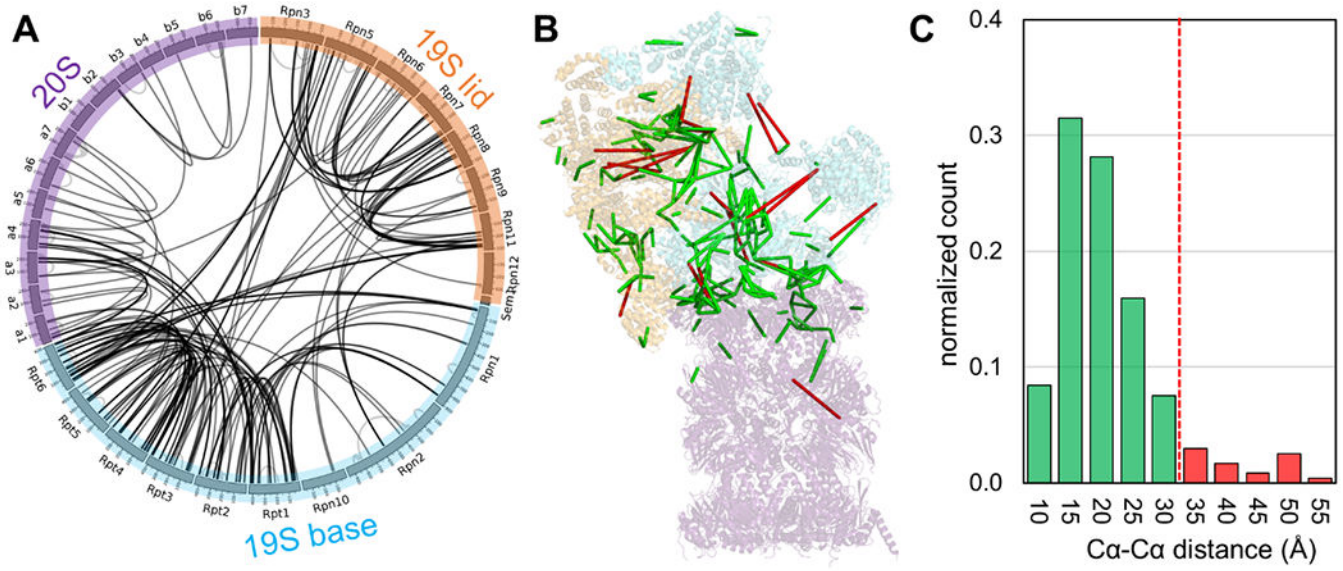

Figure 4. XL-MS data of the 26S proteasome.

(A) 2-D cross-link map generated from CX-Circos (http://cx-circos.net) depicting interconnectivity of proteasome subunits within respective subcomplexes. **(B)** Mapping of cross-links to high-resolution 26S proteasome structure (PDB 5GJR). Cross-links with mapped Cα-Cα distances below 30 Å shown in green, and above 30 Å shown in red. **(C)** Histogram showing distribution of mapped cross-links by distance.

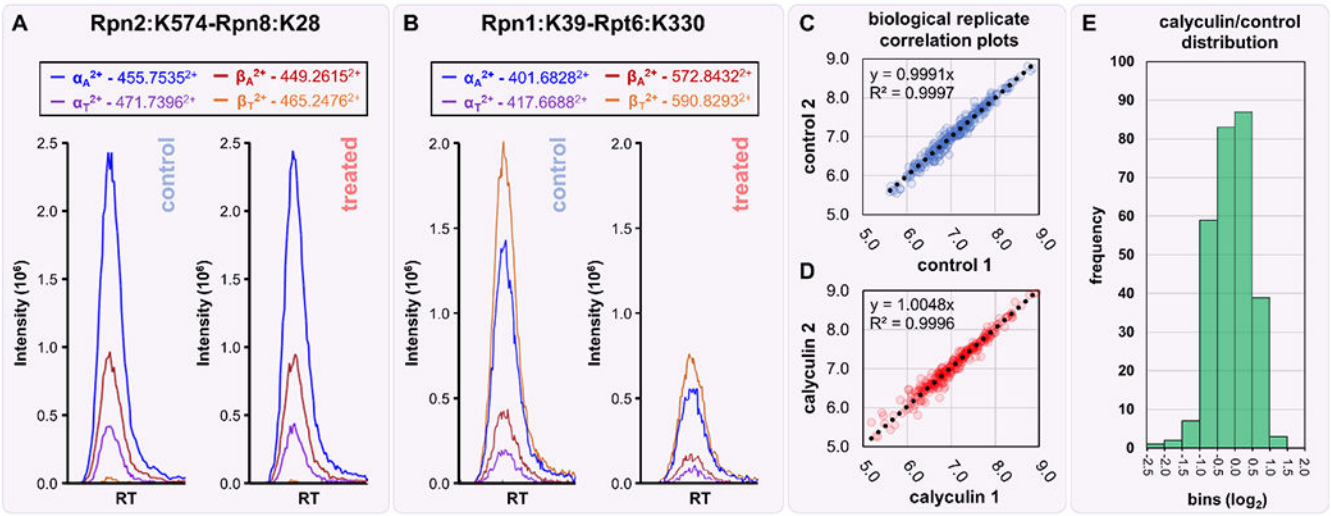

Figure 5. PRM quantitation of the proteasome cross-link targets.

PRM quantitation in Skyline for cross-link targets corresponding to **(A)** Rpn2:K574-Rpn8:K28 and **(B)** Rpn1:K39-Rpt6:K330. Four transition ions (α_A^{2+}, α_T^{2+}, β_A^{2+}, and β_T^{2+}) for each cross-link target were measured to calculate relative cross-link abundances. Pair-wise correlation plots for K-K linkage abundances between **(C)** control replicates and **(D)** calyculin-treated replicates. **(E)** Distribution of cross-link abundance ratios in calyculin-treated versus control proteasomes.

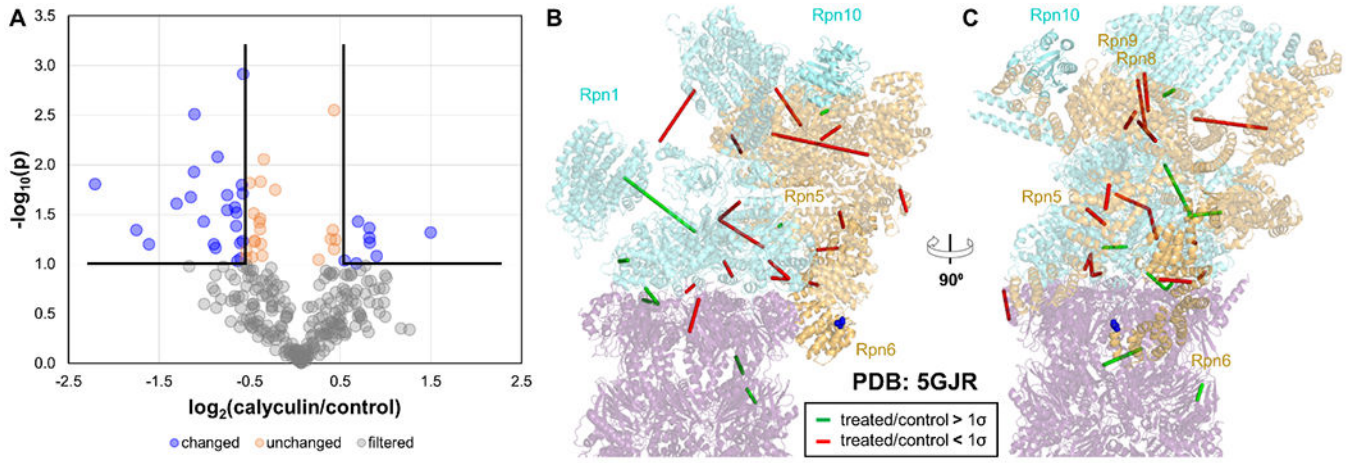

Figure 6. Analysis of statistically changed cross-links and mapping to the proteasome structure.

(A) Volcano plot depicting the distribution of changed (blue) and unchanged (orange) cross-links in treated versus control proteasome purifications. Cross-links that did not meet the p-value threshold of 0.10 are shown in gray. **(B, C)** Mapping of calyculin-dependent cross-links to high-resolution 26S proteasome structure (PDB 5GJR). Cross-links reduced in calyculin-treated proteasomes shown in red, cross-linked increased shown in green. 19S base assembly depicted in teal, 19S lid in orange, and 20S in purple.